Received: 24 March 2019 | Revised: 23 October 2019 | Accepted: 25 October 2019

DOI: 10.1111/jce.14255

ORIGINAL ARTICLE

WILEY

Imaging of subendocardial adipose tissue and fiber orientation distributions in the human left atrium using optical coherence tomography

Theresa H. Lye PhD[1] | Charles C. Marboe MD[2] | Christine P. Hendon PhD[1]

[1]Department of Electrical Engineering, Columbia University, New York, NY

[2]Department of Pathology, Columbia University Medical Center, New York, NY

Correspondence
Christine P. Hendon, Department of Electrical Engineering, Columbia University, 500 West 120th Street, Mudd 1310, New York, NY 10027.
Email: cpf2115@columbia.edu

Disclosures: None.

Funding information
National Institutes of Health, Grant/Award Number: 1DP2HL127776-01; National Science Foundation, Grant/Award Number: 1454365; Sheldon Weinig Scholars Program; Columbia University, Grant/Award Number: Presidential Fellowship

Abstract

Background: Optical coherence tomography (OCT) has the potential to provide real-time imaging guidance for atrial fibrillation ablation, with promising results for lesion monitoring. OCT can also offer high-resolution imaging of tissue composition, but there is insufficient cardiac OCT data to inform the use of OCT to reveal important tissue architecture of the human left atrium. Thus, the objective of this study was to define OCT imaging data throughout the human left atrium, focusing on the distribution of adipose tissue and fiber orientation as seen from the endocardium.

Methods and Results: Human hearts (n = 7) were acquired for imaging the left atrium with OCT. A spectral-domain OCT system with 1325 nm center wavelength, 6.5 μm axial resolution, 15 μm lateral resolution, and a maximum imaging depth of 2.51 mm in the air was used. Large-scale OCT image maps of human left atrial tissue were developed, with adipose thickness and fiber orientation extracted from the imaging data. OCT imaging showed scattered distributions of adipose tissue around the septal and pulmonary vein regions, up to a depth of about 0.43 mm from the endocardial surface. The total volume of adipose tissue detected by OCT over one left atrium ranged from 1.42 to 28.74 mm^3. Limited fiber orientation information primarily around the pulmonary veins and the septum could be identified.

Conclusion: OCT imaging could provide adjunctive information on the distribution of subendocardial adipose tissue, particularly around thin areas around the pulmonary veins and septal regions. Variations in OCT-detected tissue composition could potentially assist ablation guidance.

KEYWORDS
atrial fibrillation, imaging, left atrium, modeling, optical coherence tomography

1 | INTRODUCTION

The success of ablation for atrial fibrillation is still suboptimal, with overall, single-procedure, long-term success rates of radiofrequency ablation for atrial fibrillation having been estimated to be about 50%.[1] There exists a need for improving the guidance of ablation therapy, with remaining challenges including establishing lesion permanence and identifying optimal ablation targets within the structural substrate. In recent years, optical coherence tomography (OCT) has been demonstrated to have the potential to provide

real-time imaging guidance during ablation through the use of OCT-integrated catheters. OCT imaging has been able to distinguish ablation lesions from untreated tissue, as well as identify disruptions in the myocardium and endocardium indicative of overtreatment.[2-5] Preliminary in vivo imaging studies have captured OCT images of endocardial and myocardial features within beating swine hearts.[3,6]

In addition to tracking lesion formation, however, OCT could provide valuable information on tissue architecture by high-resolution imaging of the atrial wall. Various tissue types in the human heart, including endocardial connective tissues, myocardium, adipose tissue, and fibrotic tissue have been identified with OCT.[7-10] OCT has been shown to provide detailed imaging of interstitial collagen patterns within the myocardium.[11] However, these studies focused on small regions of tissue, which provide an incomprehensive view of the utility of OCT imaging throughout a cardiac chamber. Therefore, the objective of this study was to provide OCT data throughout the human left atrium, as imaged from the endocardium, with particular focus on the distribution of subendocardial adipose tissue and fiber orientation.

2 | MATERIALS AND METHODS

2.1 | Tissue acquisition

Whole, diseased human hearts (n = 7) were acquired under an approved protocol from the National Disease Research Interchange for imaging. The inclusion criteria for the protocol was based on the following diagnoses: end-stage heart failure, cardiomyopathy, coronary heart disease, amyloid, atrial fibrillation, and myocardial infarction. All specimens were deidentified and considered not human subjects research, according to the Columbia University Institutional Review Board Under 45 CFR 46. Donor characteristics are provided in Table 1. The average age was 63.4 years. One donor had a history of atrial fibrillation, four had congestive heart failure, two had a myocardial infarction, and one had valvular heart disease.

2.2 | Imaging protocol

The dissection, imaging, histology, and OCT image stitching protocols were carried out as described in a prior study,[11] but will be briefly summarized here with any differences noted. The left atrium was first separated from all other chambers of the human heart. For dissection, the left atrium was cut in half, separating the right pulmonary veins from the left pulmonary veins, and each pulmonary vein was then cut open longitudinally to flatten the tissues. Imaging of the left atrial appendage was excluded from this study. The tissues were imaged fresh while submerged in a 10:1 phosphate-buffered saline solution using the TELESTO I (Thorlabs GmbH, Dachau, Germany) spectral-domain OCT system, which has an axial resolution of 6.5 μm, lateral resolution of 15 μm, imaging depth of 2.51 mm in air, and a center wavelength of 1325 nm. The OCT-IMM3 immersion-style sample z-Spacer (Thorlabs GmbH) was used to image the tissues while they were submerged in a phosphate-buffered saline solution, which was done to ensure the tissues remained hydrated throughout the imaging session. Overlapping, 3D image volumes were obtained to cover the left atrium endocardium. After imaging, Trichrome histology was obtained to correlate OCT image features to tissue composition. Finally, large-scale imaging maps were developed through manual image registration and stitching. Multiband blending, and when necessary, gain compensation, were carried out as described in a prior study.[12]

2.3 | Adipose tissue volume and fiber orientation extraction

Adipose tissue was manually segmented with IMOD[13] in each en face OCT image. The presence of adipose was determined by a brightly spotted or "honeycomb" pattern, typically with a background of decreased intensity than surrounding myocardium. Adipose thickness was determined by summing the segmented voxels in the axial direction and converting the summed values to real dimensions based on the axial resolution. Based on the segmentation in the OCT images, overall imaged adipose tissue volume was computed for each left atrium. Additionally, because the septum in particular was found to contain significant adipose regions, the adipose tissue volume in only the septum region was computed.

To examine overall fiber orientation trends over large regions, fiber orientation was demarcated manually based on visual striations observed within the en face OCT images. While myofiber orientation in the left atrium changes over depth, and OCT imaging is capable of providing high-resolution imaging of transmural changes as previously demonstrated,[11] fiber orientation was not observed to change significantly within the imaging depth of OCT for the majority of regions in the human left atrium. Therefore, fiber orientation was identified from a single representative depth.

2.4 | Model registration

Registration of white light and en face OCT images to a 3D left atrium model was carried out to facilitate the interpretation of image

TABLE 1 Donor information

Heart #	Age	Sex	Cardiovascular disease history
1	77	F	CAD, HTN, CHF, AF, PVD
2	70	F	CHF, HTN
3	46	F	HTN, CAD, MI
4	67	M	MI, HTN, HLD
5	59	F	HTN
6	67	M	CHF, VHD, HLD
7	58	M	CAD, CHF, HTN, HLD

Abbreviations: AF, atrial fibrillation; CAD, coronary artery disease; CHF, congestive heart failure; F, female; HLD, hyperlipidemia; HTN, hypertension; M, male; MI, myocardial infarction; PVD, peripheral vascular disease; VHD, valvular heart disease.

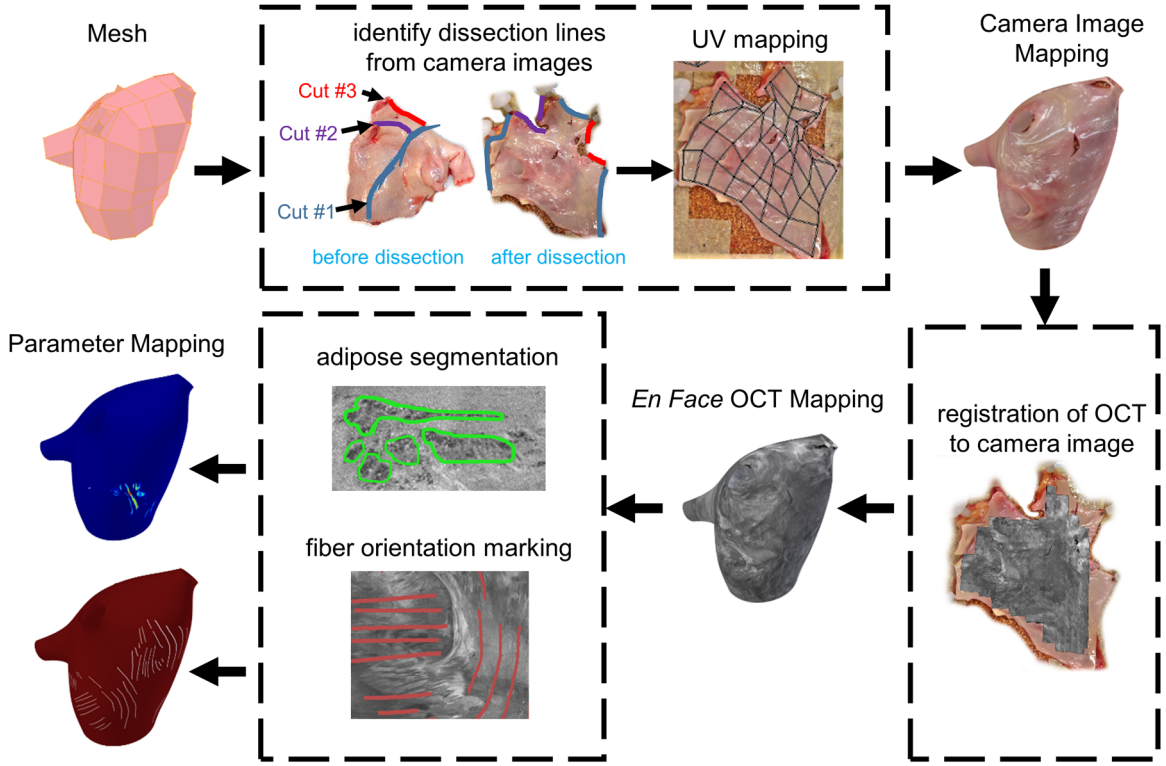

FIGURE 1 Overview of registration of optical coherence tomography (OCT) image maps to the 3D model

features of dissected tissue with respect to overall left atrial anatomy. Registration was carried out in the open-source, 3D computer graphics software Blender. The registration procedure is depicted in Figure 1. A 3D left atrium model from the Continuity 6 online database, developed by the Cardiac Mechanics Research Group of the University of California San Diego, was used as a reference left atrium model.[14]

White light images were mapped to the model first because anatomical landmarks used for registration could be more easily identified in the white light images as opposed to the OCT images. Knowledge of the location of cuts made during dissection, as well as anatomical landmarks, such as the pulmonary veins and left atrial appendage, facilitated the wrapping of the white light images of the dissected tissues back into a 3D form. The mapping was carried out using Blender's UV mapping interface, where white light images were manually registered to the appropriate faces of the mesh. To provide a smooth visualization, histogram equalization and illumination correction were carried out for the white light images of each heart. Illumination correction was accomplished by converting the white light images from red, green, blue (RGB) to the hue, saturation, value (HSV) domain. Within the HSV domain, the overall average illumination, calculated as the average of the V channel, was computed over the entire white light image. Regional illumination was then computed by Gaussian filtering the V channel with a 200×200 kernel and a 100-pixel standard deviation. The regional illumination was replaced by the uniform, average illumination by subtracting the Gaussian filtered V channel from the original V channel and adding the overall average of the original V channel. The white light images were then registered to the model, and seams in the texture maps from UV mapping were smoothed in Blender. The same model was used for all hearts, although slight adjustments to the size and shape of the model were made to more appropriately suit each heart.

After the white light images were registered to the model, OCT en face images could be manually registered to the white light images based on anatomical landmarks and the shape of the imaged region, and then subsequently registered to the model with an identical procedure. The en face OCT images simply replace the texture data of the model in lieu of the white light images. Similarly, any parameter maps derived from the OCT images, such as adipose tissue thickness and fiber orientation, could be registered to the 3D model with the same approach.

3 | RESULTS

Endocardial thickness and composition, distributions of adipose tissue, and fiber directionality were visible within OCT imaging data of the human left atria. Endocardial thickness varied over the left atrium, and varying densities and compositions of connective tissue within the endocardium could be observed in OCT as different layers and variations in intensity, as has been described previously.[7,11] Endocardial thickness was typically thinner near the septum, which allowed the septal region to be particularly feature-rich within the imaging depth of OCT. Adipose tissue and fiber orientation were often visible within the septal region. Notably, the

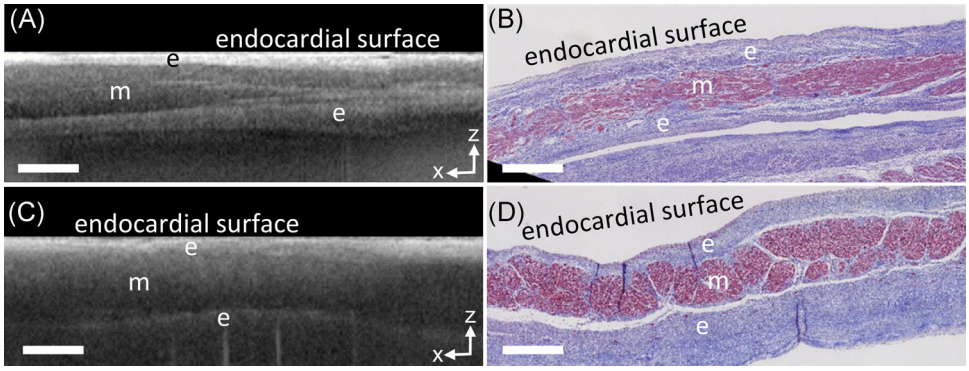

FIGURE 2 Structures at the septum, as viewed from the endocardial side of the left atrium, imaged transmurally by optical coherence tomography (OCT). A, OCT b-scan of the septum primum. B, Corresponding histology to A. C, OCT b-scan at the fossa ovalis. D, Corresponding histology to C. Scale bars indicate 0.5 mm. e, endocardium, m, myocardium

full thickness of the septum primum could be imaged by OCT in thin regions, as shown in Figure 2. At the endocardial surface in the OCT images of Figure 2, a thin, bright layer representing the endocardium is seen, followed by a lower intensity region underneath representative of the myocardium. Deeper within the tissue, a higher intensity layer compared to the myocardium is present once more, representative of the endocardium at the opposing side of the myocardium.

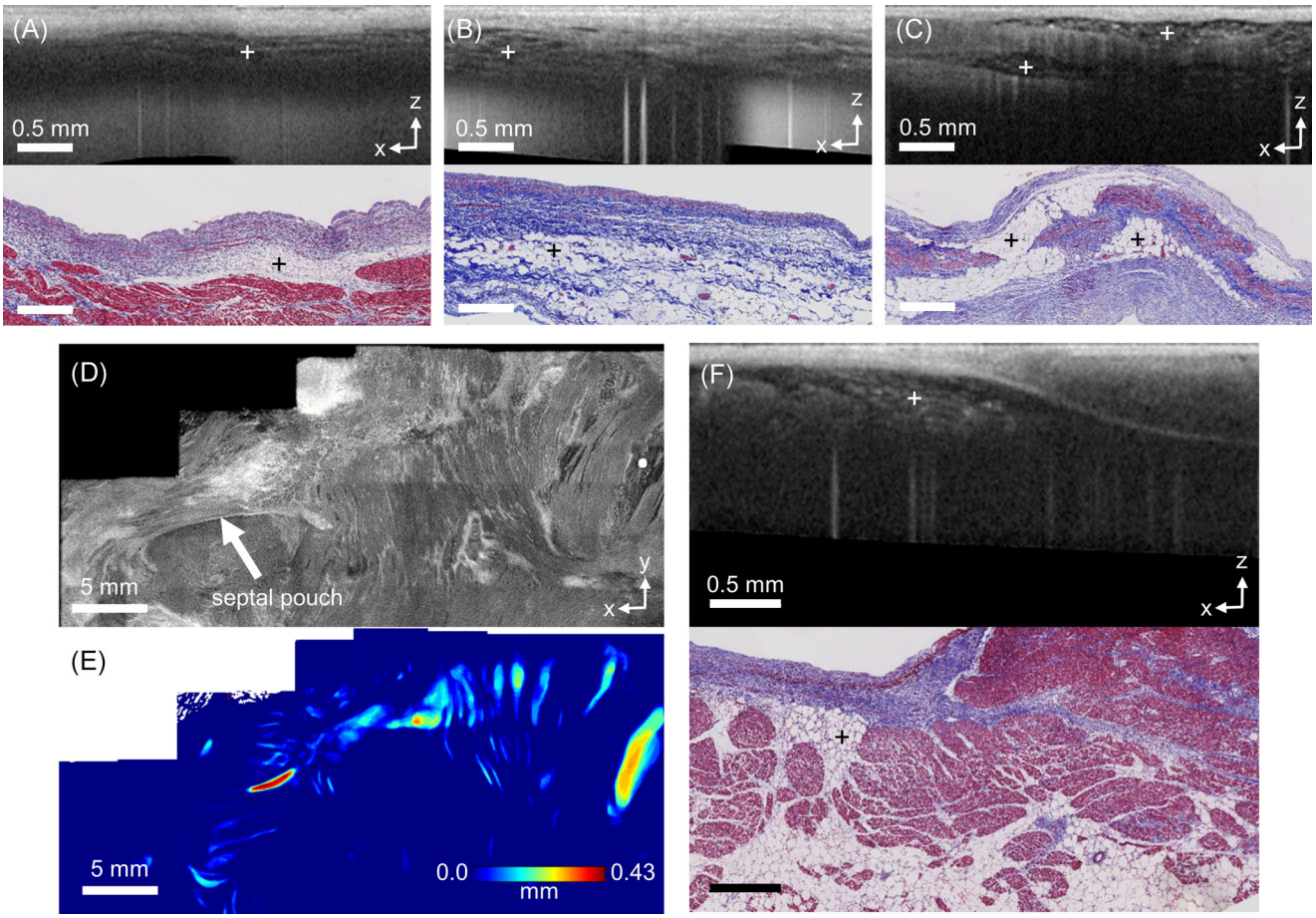

FIGURE 3 Adipose distributions in human left atrial tissue, as imaged by optical coherence tomography (OCT). A, OCT B-scan (top) and histology (bottom) of adipose overlying a myocardial sleeve in a pulmonary vein. B, OCT B-scan (top) and histology (bottom) of adipose tissue from the fibrofatty adventitia. C, OCT B-scan (top) and histology (bottom) of adipose tissue in the septum primum. D, En face OCT image around the fossa ovalis (top), shown 0.26 mm from the endocardial surface, showing adipose tissue distributed over a wide area. The white dot in the en face OCT image corresponds to the location of the B-scan shown in F. E, Corresponding adipose thickness map to D. F, OCT B-scan (top) and histology (bottom) of adipose near the fossa ovalis. The crosses mark the areas of adipose tissue

3.1 | Adipose features

Adipose tissue is highly recognizable within OCT images with a distinct "honeycomb" texture that can also become a speckled or brightly dotted texture if farther from the imaging focus. All following descriptions of adipose tissue, including their measurements of thickness and volume, pertain to the adipose tissue imaged by OCT and visible within OCT's imaging depth unless otherwise specified. Within the OCT imaging data throughout the human left atrium, adipose tissue could typically be observed in specific locations, which are summarized in Figure 3. Adipose tissue was seen in a thin layer underneath the venous media and above the myocardium within the myocardial sleeves, shown in Figure 3A, as well as in the fibrofatty adventitia of the pulmonary veins as seen in Figure 3B. Adipose tissue was also markedly visible around the septum. Subendocardial adipose tissue could exist in large pockets that transmurally spanned the atrial wall in thinner regions of the septum primum, shown in Figure 3C, and was particularly prominent near regions where a septal pouch[15] could be seen. More generally, subendocardial adipose tissue could be seen distributed around the septal region in small pockets of varying sizes, as demonstrated in the en face OCT image of Figure 3D and corresponding adipose tissue thickness map of Figure 3E. These adipose pockets were seen to be located directly underneath the endocardium within OCT, although histology showed that adipose directly underneath the endocardium could be connected to larger volumes of adipose tissue as shown in Figure 3F.

The amount of adipose tissue as imaged by OCT was variable among hearts, particularly around the septum due to a large amount of adipose tissue potentially observed there. The total thickness and volume of adipose captured by OCT across left atria is provided in Table 2. The maximum thickness of adipose tissue, about 0.4 mm, was typically limited by the imaging depth of OCT. Note that variability in total adipose tissue volume over the whole heart could depend on the length of the pulmonary veins that were still intact upon heart acquisition, which varied from specimen to specimen. However, the total volume of adipose tissue specifically around the region of the septum also varied greatly.

TABLE 2 Adipose Measurements

Heart #	Max thickness, mm	Total volume, mm^3	Total volume at septum, mm^3
1	0.36	4.82	4.82
2	0.26	2.01	1.69
3	0.43	9.84	[a]
4	0.42	18.10	5.69
5	0.38	11.77	7.52
6	0.40	28.74	11.57
7	0.20	1.42	1.26

[a]The entire septum region could not be appropriately identified in Heart #3, and thus was excluded.

Representative registrations of adipose tissue thickness map to the left atrium model are shown in Figure 4. As described previously, adipose tissue was seen primarily around the septum and was especially thick near the septal pouch. This region tended to have the largest continuous areas of adipose tissue and contributed significantly to the volume of adipose tissue around the septum. There were also some distributions of adipose around the pulmonary veins. Adipose tissue more distant from these two locations was only observed in heart #6, shown in Figure 4E, which showed significant amounts of adipose tissue spanning a large distance of the left atrial wall superior to the left atrial appendage. Correlated histology and OCT b-scans throughout heart #6 are provided in Figure S2 to provide further comparisons between OCT and histology. It was noted in heart #5 that regions of abundant adipose and connective tissue at the septum were visible from gross inspection of the endocardial surface and could be imaged in more detail with OCT. This is shown in Figure 5, where OCT was able to visualize pockets of adipose, as well as bright patches and striations corresponding to connective tissue.

3.2 | Fiber orientation features

Representative mappings of fiber orientation, as extracted from manual measurements to the 3D left atrial model are presented in Figure 6. A representative example of an OCT en face image displaying fiber orientation is given in the Figure S3, showing the striations indicative of fiber orientation. Given OCT's imaging depth, fiber orientation information could most often be extracted from the septal region and around the pulmonary veins. Consistent with findings from gross inspection and DT-MRI, fibers often wrapped circumferentially around the pulmonary vein ostia.[16,17] Within hearts #5 and #6, fiber orientation wrapping around the right pulmonary veins with obliquely running fibers between the pulmonary veins and fiber orientation circumferential to the waist of the left atrium underneath, as seen on the far right in Figure 6D,E, is also consistent with observations from DT-MRI data.[16]

4 | DISCUSSION

To the authors' knowledge, this study is the first to present OCT imaging data throughout the human left atrium on a large scale. Prior OCT imaging studies in the human heart focused on small regions of tissue and did not map the distribution of imaged tissue features throughout an entire cardiac chamber. Within this study, the distribution of adipose tissue and fiber orientation throughout the human left atrium, as seen from imaging from the endocardium, were presented through mapping of large scale, stitched OCT imaging maps to a human left atrial model.

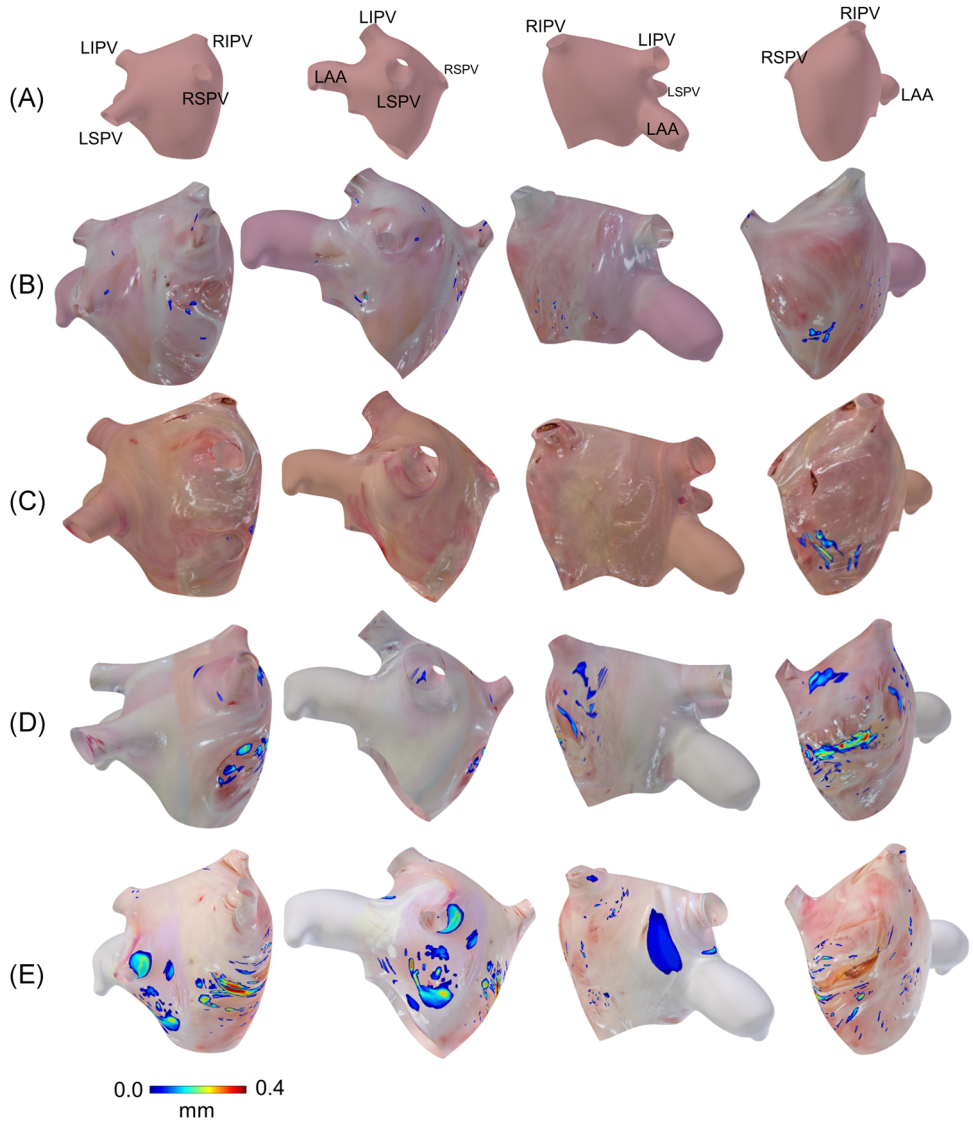

FIGURE 4 Adipose thickness distributions in the human left atria, as extracted from optical coherence tomography (OCT) images and superimposed on 3D anatomical models. The adipose thickness is shown as a color map, while areas where adipose was not seen instead show camera images of the left atrial tissue. The models are shown in four views. A, Reference model, showing the location of the pulmonary veins and left atrial appendage relative to the view. Note that the left atrium is inverted, such that the endocardial surface faces outwards. B, Adipose thickness distribution from heart #7. C, Adipose thickness distribution from heart #1. D, Adipose thickness distribution from heart #5. E, Adipose thickness distribution from heart #6. Adipose thickness distributions for hearts #2 and #4 are given in the Figure S1. LAA, left atrial appendage; LIPV, left inferior pulmonary vein; LSPV, left superior pulmonary vein; RIPV, right inferior pulmonary vein; RSPV, right superior pulmonary vein

4.1 | Applications of OCT-integrated catheter imaging to tissue structure characterization

Several studies have demonstrated the development of OCT-integrated catheters that may be useful for ablation guidance, in vivo. With OCT's video-rate imaging speeds and high resolution, these studies have focused on the application of using OCT-integrated catheters to monitor ablation lesion formation in real-time.[3-6,18,19] In addition to imaging lesions, OCT-integrated catheters could simultaneously provide a real-time, high-resolution characterization of the left atrial tissue structure. However, there exists a lack of OCT data over the human left atrium to inform this application.

This study provides information on the distribution of adipose tissue and fiber orientation that can be imaged by OCT throughout the human left atrium. Imaging of tissue features is limited by the thickness of the endocardium. For this reason, most adipose tissue and fiber orientation features could be identified around the pulmonary veins and septal regions where the tissue thickness is thinner. Distributed pockets of subendocardial adipose tissue could be observed around the septal region of the left atrium. OCT was also able to identify the full thickness of the septum primum in thin areas.

Based on these results, OCT may provide adjunctive tissue structure information in the in vivo setting regarding endocardial

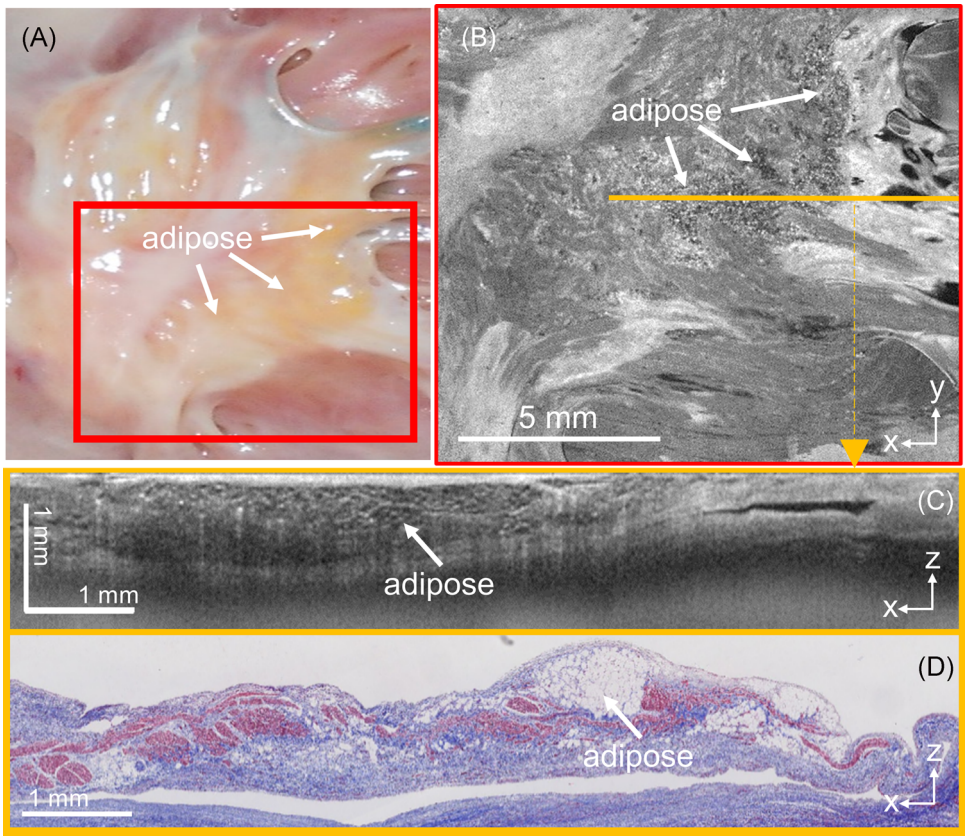

FIGURE 5 Representative example of significant amounts of interstitial, subendocardial adipose at the septum primum, as imaged by optical coherence tomography (OCT). A, Camera image of region of interest. B, En face OCT image of the region depicted in the red box in A. C, OCT b-scan corresponding to the location of the orange line in B. D, Corresponding histology to C

thickness, the presence of adipose tissue directly underneath the endocardium, and identification of thin-walled regions. Due to the limited fiber orientation information visible within the imaging depth of OCT and the difficulty of mapping precisely in a beating heart, mapping of fiber orientation with OCT may be difficult in an in vivo setting without further improvements. However, it is possible that variations in OCT-detected tissue composition at the point of catheter-tissue contact may have an effect on ablation lesion formation or electrogram measurements due to differences in tissue biophysical properties.

4.2 | Ex vivo and in vivo OCT imaging

In vivo, OCT-integrated catheter imaging has been carried out in live swine hearts, demonstrating the ability of OCT to visualize endocardial, myocardial, and ablated tissue features in blood within beating hearts.[3,6] However, imaging of adipose tissue, as shown in this study, has not yet been imaged in vivo, with prior in vivo OCT imaging studies focusing on imaging the formation of ablation lesions. It is likely that differences in image quality will be introduced when translating to an in vivo, catheter-based design. Imaging resolutions comparable to the resolutions within this study, however, were achieved in the previously demonstrated OCT-integrated catheter, which had 15 μm resolution with an imaging speed of 10 frames per second and 4500 A-lines per frame.[6] Imaging of adipose tissue with an OCT-integrated catheter in the ex vivo setting is also provided in Figure S4, demonstrating the visualization of adipose with catheter-based imaging. In the in vivo setting, the tissue will also be in contact with a glass cover, similar to the immersion lens used with the benchtop system of this study. The most significant change will likely be the mapping mechanism for obtaining a visualization over broad regions of the human left atrium. In this study, the tissues were flattened, with overlapping OCT image volumes obtained over the tissues and stitched together into large image maps. In an in vivo setting, this would be not possible. One possibility for in vivo substrate characterization with OCT is to rapidly analyze OCT images obtained at tissue contact for tissue composition and then register this information with electroanatomic mapping. Thus, parametric maps representing tissue composition can be visualized on chamber geometry, similar to the mapping of voltage measurements during electroanatomic mapping. This approach will require translation of OCT tissue type classification algorithms[7,20] to real-time.

4.3 | Comparison of OCT to other high-resolution imaging modalities

High resolution, catheter imaging has also been demonstrated with confocal microscopy in situ in dog hearts, where atrial and ventricular myocardium, blood flow, and fibrosis were imaged with a lateral

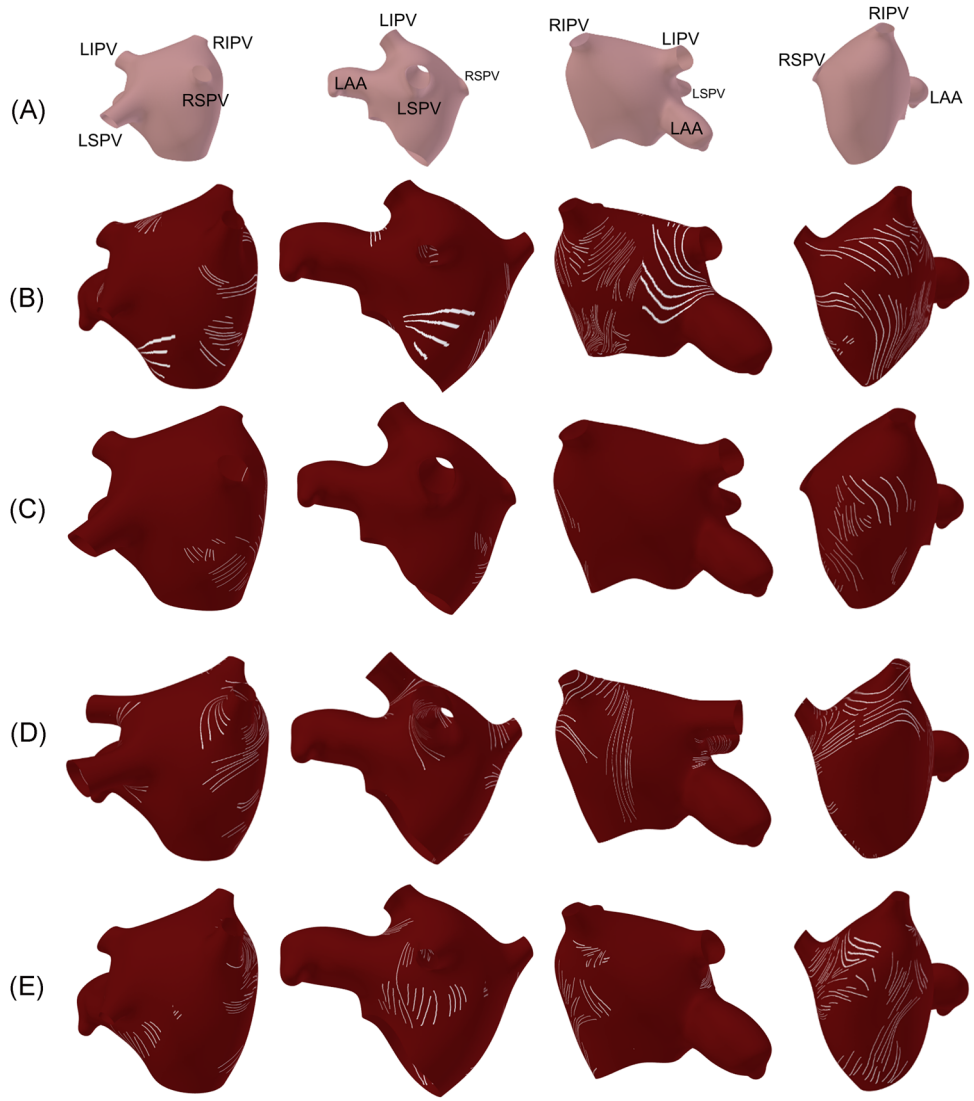

FIGURE 6 Fiber orientation in the human left atria, as extracted from optical coherence tomography (OCT) images and superimposed on 3D anatomical models. A, Reference model, showing the location of the pulmonary veins and left atrial appendage relative to the view. Note that the left atrium is inverted, such that the endocardial surface faces outwards. B, Fiber orientation from heart #7. C, Fiber orientation distribution from heart #1. D, Fiber orientation distribution from heart #5. E, Fiber orientation distribution from heart #6. Fiber orientation distributions for hearts #2 and #4 are given in Figure S1. LAA, left atrial appendage; LIPV, left inferior pulmonary vein; LSPV, left superior pulmonary vein; RIPV, right inferior pulmonary vein; RSPV, right superior pulmonary vein

resolution of 1.4 μm and axial resolution of 9 μm. The microprobes were able to acquire images with 244 by 255 μm field of views and imaging depths of 66 μm.[21] However, OCT imaging provides information on a different scale, with a millimeter field of view compared to the micrometer field of views offered by confocal microscopy.

In recent years, high-resolution magnetic resonance imaging (MRI) and computed tomography (CT) imaging modalities have enabled the acquisition of detailed tissue architecture in the ex vivo setting. Transmural fiber orientation has been imaged over the whole, fixed human atria using diffusion tensor MRI with a resolution of $500 \times 500 \times 1000\,\mu m^3$, which was reconstructed to $400\,\mu m^3$ resolution.[16] Imaging of fibrosis, fat and fatty fibrosis in human left atrial tissue has also been accomplished using saturation recovery T1 mapping and DIXON MRI imaging with resolutions of $200 \times 200 \times 1000\,\mu m^3$.[22] 3D gadolinium-enhanced MRI in human right atrial tissue has imaged interstitial fibrosis and transmural fiber orientation with $80\,\mu m^3$ resolution.[23] Contrast-enhancement MRI has imaged fibrosis and fiber orientation within whole human atria with $180 \times 180 \times 360\,\mu m^3$ resolution.[24] Micro CT has also been used to extract myofiber orientation from human atria at a resolution of $49\,\mu m^3$,[25] and from the whole heart with $73\,\mu m^3$ resolution.[26] As demonstrated in these studies, high-resolution MRI and CT can provide detailed information throughout the entire cardiac chamber, particularly on fiber orientation and fibrosis. Compared to these imaging modalities, OCT offers an adjunctive imaging approach with increased resolution and the potential for real-time, in vivo imaging directly from the ablation catheter. OCT is more likely to provide

real-time information on tissue composition such as adipose tissue and endocardial thickness, which may enable insights on measurements obtained at the catheter location. The OCT system utilized within this study provides an imaging resolution of $15 \times 15 \times 6.5\ \mu m^3$, and in general, OCT imaging resolutions may range from about 1 to 15 μm.[27]

4.4 | Future applications of cardiac OCT

While this study focused on adipose tissue and fiber orientation, it is also possible for OCT to provide features corresponding to fibrosis, as has been described in prior OCT studies.[8,11] Previously, OCT has also been used to describe myofiber orientation within animal models, ex vivo,[28-37] with some studies incorporating optical clearing[30,34] or serial sectioning[37] methods to improve imaging depth. Polarization-sensitive OCT, which provides additional contrast by measuring changes in the polarization state of light as it passes through a medium,[38] has also been used to provide additional sensitivity to fiber organization.[31,35,36] OCT imaging of myofiber orientation in mouse hearts has been used to describe changes in fiber organization with respect to cardiomyopathy,[33] infarction[34] and aging.[37] While it was shown in this study that tissue features could only be identified by OCT in shallow regions under thin endocardium, the use of optical clearing or serial sectioning could make it possible to generate highly detailed, transmural, large scale image maps for understanding myofiber structure and adipose distributions in the ex vivo setting. The tissue structure information obtained from OCT imaging could also be incorporated into tissue-specific models to further probe the influences of tissue microstructure on electrophysiological patterns.[39]

4.5 | Limitations

This study was carried out ex vivo, and while in vivo imaging with OCT-integrated catheters has been previously demonstrated,[3,6] further studies and development would be needed to confirm applicability to clinical use. Additionally, without further processing of the tissue, OCT is only able to characterize features near the surface. In this study, adipose tissue thickness measurements only corresponded to adipose within the imaging depth of OCT. Thus, the true adipose tissue thickness through the entire atrial wall would be larger in some areas than measured from OCT imaging. Additionally, comparisons of OCT to larger, annotated histology maps are needed to quantify the accuracy of tissue feature maps extracted from OCT. While the majority of the left atrial tissue was imaged, some regions at the edges of the dissected tissues were not imaged due to the manual nature of image acquisition and limitations of the imaging setup. This left some unimaged areas, especially along the central dissection line between the left and right pulmonary veins, and therefore it is possible that the amount of useful OCT image features over the human left atrium was underestimated. Furthermore, a single left atrial model was used to approximate the location of imaged features within human left atrial anatomy. However, the size and morphology of human hearts differ, and more precise mapping would require personalized models of the left atria, such as could be obtained from MRI or CT. Finally, in the future, characterization of other image features of interest, such as endocardial thickness and fibrosis could be further investigated and quantified.

5 | CONCLUSION

This study demonstrated the first OCT imaging throughout the human left atrium with respect to left atrial anatomy and showed that OCT can provide quantification of adipose tissue and fiber orientation, particularly near the septal region and pulmonary veins. The structural information provided by OCT could assist in ablation guidance, in addition to lesion formation monitoring.

ACKNOWLEDGMENTS

The authors would like to thank Dr. Yu Gan for assistance with the image registration and stitching algorithm, as well as Dr. Andrew McCulloch and Dr. Kevin Vincent for their expertise on modeling. This work was supported by the National Institutes of Health 1DP2HL127776-01 (CPH), National Science Foundation Career Award 1454365 (CPH), the Columbia University Fu Foundation School of Engineering and Applied Science Presidential Fellowship (THL), and the Sheldon Weinig Scholars Program (THL).

AUTHOR CONTRIBUTIONS

CPH conceived the research aims and secured funding. THL collected, processed, and analyzed the data. CCM interpreted the data and results. THL drafted the article, while CPH and CCM provided feedback, revised, and approved the article.

ORCID

Theresa H. Lye http://orcid.org/0000-0001-7310-4220
Christine P. Hendon http://orcid.org/0000-0001-7318-1517

REFERENCES

1. Ganesan AN, Shipp NJ, Brooks AG, et al. Long-term outcomes of catheter ablation of atrial fibrillation: a systematic review and meta-analysis. *J Am Heart Assoc*. 2013;2(2):e004549.
2. Fleming CP, Quan KJ, Wang H, Amit G, Rollins AM. In vitro characterization of cardiac radiofrequency ablation lesions using optical coherence tomography. *Opt Express*. 2010;18(3):3079-3092.
3. Fleming CP, Rosenthal N, Rollins AM, Arruda MM. First in vivo real-time imaging of endocardial radiofrequency ablation by optical coherence tomography: implications on safety and the birth of "electro-structural" substrate-guided ablation. *J Innov Card Rhythm Manag*. 2011;2:199-201.
4. Zhao X, Fu X, Blumenthal C, et al. Integrated RFA/PSOCT catheter for real-time guidance of cardiac radio-frequency ablation. *Biomed Opt Express*. 2018;9(12):6400-6411.

5. Liang D, Taeschler D, Goepfert C, et al. Radiofrequency ablation lesion assessment using optical coherence tomography - a proof-of-concept study. *J Cardiovasc Electrophysiol*. 2019;30(6):934-940.
6. Wang H, Kang W, Carrigan T, et al. In vivo intracardiac optical coherence tomography imaging through percutaneous access: toward image-guided radio-frequency ablation. *J Biomed Opt*. 2011;16(11):110505.
7. Gan Y, Tsay D, Amir SB, Marboe CC, Hendon CP. Automated classification of optical coherence tomography images of human atrial tissue. *J Biomed Opt*. 2016;21(10):101407.
8. Yao X, Gan Y, Ling Y, Marboe CC, Hendon CP. Multicontrast endomyocardial imaging by single-channel high-resolution cross-polarization optical coherence tomography. *J Biophotonics*. 2018;11(4):e201700204.
9. Gan Y, Lye TH, Marboe CC, Hendon CP. Characterization of the human myocardium by optical coherence tomography [published online ahead of print August 9, 2019]. *J Biophotonics*. 2019:e201900094.
10. Hendon CP, Lye TH, Yao X, Gan Y, Marboe CC. Optical coherence tomography imaging of cardiac substrates. *Quant Imaging Med Surg*. 2019;9(5):882-904.
11. Lye TH, Iyer V, Marboe CC, Hendon CP. Mapping the human pulmonary venoatrial junction with optical coherence tomography. *Biomed Opt Express*. 2019;10(2):434-448.
12. GanY, YaoW, MyersKM, VinkJY, WapnerRJ, HendonCP. Analyzing three-dimensional ultrastructure of human cervical tissue using optical coherence tomography. *Biomed Opt Express*. 2015;6(4):1090-1108.
13. Kremer JR, Mastronarde DN, McIntosh JR. Computer visualization of three-dimensional image data using IMOD. *J Struct Biol*. 1996;116(1):71-76.
14. Gonzales MJ, Sturgeon G, Krishnamurthy A, et al. A three-dimensional finite element model of human atrial anatomy: new methods for cubic Hermite meshes with extraordinary vertices. *Med Image Anal*. 2013;17(5):525-537.
15. Holda MK, Koziej M, Holda J, et al. Atrial septal pouch - Morphological features and clinical considerations. *Int J Cardiol*. 2016;220:337-342.
16. Pashakhanloo F, Herzka DA, Ashikaga H, et al. Myofiber architecture of the human atria as revealed by submillimeter diffusion tensor imaging. *Circ Arrhythm Electrophysiol*. 2016;9(4):e004133.
17. Ho SY, Sanchez-Quintana D, Cabrera JA, Anderson RH. Anatomy of the left atrium: implications for radiofrequency ablation of atrial fibrillation. *J Cardiovasc Electrophysiol*. 1999;10(11):1525-1533.
18. Fu X, Wang Z, Wang H, Wang YT, Jenkins MW, Rollins AM. Fiber-optic catheter-based polarization-sensitive OCT for radio-frequency ablation monitoring. *Opt Lett*. 2014;39(17):5066-5069.
19. Fleming CP, Wang H, Quan KJ, Rollins AM. Real-time monitoring of cardiac radio-frequency ablation lesion formation using an optical coherence tomography forward-imaging catheter. *J Biomed Opt*. 2010;15(3):030516.
20. Yao X, Gan Y, Chang E, Hibshoosh H, Feldman S, Hendon C. Visualization and tissue classification of human breast cancer images using ultrahigh-resolution OCT. *Lasers Surg Med*. 2017;49(3):258-269.
21. Huang C, Wasmund S, Hitchcock R, Marrouche NF, Sachse FB. Catheterized fiber-optics confocal microscopy of the beating heart in situ. *Circ Cardiovasc Imaging*. 2017;10(10):e006881.
22. Bouazizi K, Rahhal A, Kusmia S, et al. Differentiation and quantification of fibrosis, fat and fatty fibrosis in human left atrial myocardium using ex vivo MRI. *PLoS One*. 2018;13(10):e0205104.
23. Hansen BJ, Zhao J, Csepe TA, et al. Atrial fibrillation driven by micro-anatomic intramural re-entry revealed by simultaneous sub-epicardial and sub-endocardial optical mapping in explanted human hearts. *Eur Heart J*. 2015;36(35):2390-2401.
24. Zhao J, Hansen BJ, Wang Y, et al. Three-dimensional integrated functional, structural, and computational mapping to define the structural "fingerprints" of heart-specific atrial fibrillation drivers in human heart ex vivo. *J Am Heart Assoc*. 2017;6(8):e005922.
25. Zhao J, Hansen BJ, Csepe TA, et al. Integration of high resolution optical mapping and 3D micro-CT imaging to resolve the structural basis of atrial conduction in the human heart. *Circ Arrhythm Electrophysiol*. 2015;8(6):1514-1517.
26. Stephenson RS, Atkinson A, Kottas P, et al. High resolution 3-dimensional imaging of the human cardiac conduction system from microanatomy to mathematical modeling. *Sci Rep*. 2017;7(1):7188.
27. Fujimoto JG, Pitris C, Boppart SA, Brezinski ME. Optical coherence tomography: an emerging technology for biomedical imaging and optical biopsy. *Neoplasia*. 2000;2(1-2):9-25.
28. Fleming CP, Ripplinger CM, Webb B, Efimov IR, Rollins AM. Quantification of cardiac fiber orientation using optical coherence tomography. *J Biomed Opt*. 2008;13(3):030505.
29. Ambrosi CM, Fedorov VV, Schuessler RB, Rollins AM, Efimov IR. Quantification of fiber orientation in the canine atrial pacemaker complex using optical coherence tomography. *J Biomed Opt*. 2012;17(7):071309.
30. Goergen CJ, Radhakrishnan H, Sakadzic S, et al. Optical coherence tractography using intrinsic contrast. *Opt Lett*. 2012;37(18):3882-3884.
31. Fan C, Yao G. Imaging myocardial fiber orientation using polarization sensitive optical coherence tomography. *Biomed Opt Express*. 2013;4(3):460-465.
32. Gan Y, Fleming CP. Extracting three-dimensional orientation and tractography of myofibers using optical coherence tomography. *Biomed Opt Express*. 2013;4(10):2150-2165.
33. Wang Y, Zhang K, Duan D, Yao G. Heart structural remodeling in a mouse model of Duchenne cardiomyopathy revealed using optical polarization tractography [Invited]. *Biomed Opt Express*. 2017;8(3):1271-1276.
34. Goergen CJ, Chen HH, Sakadžić S, Srinivasan VJ, Sosnovik DE. Microstructural characterization of myocardial infarction with optical coherence tractography and two-photon microscopy. *Physiol Rep*. 2016;4(18):e12894.
35. Wang Y, Zhang K, Wasala NB, Yao X, Duan D, Yao G. Histology validation of mapping depth-resolved cardiac fiber orientation in fresh mouse heart using optical polarization tractography. *Biomed Opt Express*. 2014;5(8):2843-2855.
36. Wang Y, Yao G. Optical tractography of the mouse heart using polarization-sensitive optical coherence tomography. *Biomed Opt Express*. 2013;4(11):2540-2545.
37. Castonguay A, Lefebvre J, Pouliot P, Avti P, Moeini M, Lesage F. Serial optical coherence scanning reveals an association between cardiac function and the heart architecture in the aging rodent heart. *Biomed Opt Express*. 2017;8(11):5027-5038.
38. de Boer JF, Hitzenberger CK, Yasuno Y. Polarization sensitive optical coherence tomography – a review [Invited]. *Biomed Opt Express*. 2017;8(3):1838-1873.
39. Lye TH, Vincent KP, McCulloch AD, Hendon CP. Tissue-specific optical mapping models of swine atria informed by optical coherence tomography. *Biophys J*. 2018;114(6):1477-1489.

SUPPORTING INFORMATION

Additional supporting information may be found online in the Supporting Information section.

How to cite this article: Lye TH, Marboe CC, Hendon CP. Imaging of subendocardial adipose tissue and fiber orientation distributions in the human left atrium using optical coherence tomography. *J Cardiovasc Electrophysiol*. 2019;30:2950–2959. https://doi.org/10.1111/jce.14255